THE NEAREST STAR: RESOLVING THE BUILDING BLOCKS OF THE CORONAL DEM

L. Lin, V. L. Kashyap, J. J. Drake, E. E. DeLuca, M. Weber, and A. L. Sette.

Smithsonian Astrophysical Observatory, 60 Garden St, Cambridge, MA 02138, U.S.A

Abstract

We have constructed differential emission measures (DEMs) of different structures in the solar corona using data from multiple instruments. We apply a sophisticated DEM reconstruction technique to solar imaging and spectral data obtained contemporaneously using Yohkoh/SXT, TRACE, SoHO/EIT, SoHO/CDS, and GOES. The method is easily adapted to any combination of observations with different instruments and filters. We employ the technique to characterize the DEM in the solar active region AR 8232 (June 1998) for which data are available from all five instruments. We compare DEMs spatially averaged over large regions with those derived for individually resolved features and discuss the results.

Key words: Corona: Emission Measure – Software: PINTofALE,MCMC

1. Introduction

Stellar coronal emission is usually understood as being similar to that on the Sun (the so-called Solar Analogy), in that stellar coronae are believed to be organized by magnetic fields and heated in the same manner as the solar corona. Despite some obvious differences in the scale and scope of the physics (e.g., the lack of a normal $\alpha - \omega$ dynamo in low-mass dMe stars), the well-known correspondence between X-ray luminosity and the Rossby number and rotation rate (see e.g., Vaiana et al. 1981, Golub 1981, Rosner et al. 1985) suggest that the Solar Analogy is a useful description, and must be explored in greater detail.

High resolution X-ray spectra from the current generation of X-ray satellites, Chandra and XMM-Newton, have made possible detailed analysis of the structure of stellar coronae, and in particular their differential emission measures. Our interpretation of these stellar emission measures is however limited in that the spectra are full-disk integrations and offer no spatial resolution. We can only speculate on what types of coronal substructures (quiescent loops, flaring plasma, post-flare loops, bright points, etc.) are principally responsible for the X-ray emission, and on the morphology of phenomena behind the emission measures we retrieve from the data.

This issue may be addressed by first examining emission measure distributions of the solar corona. The current generation of solar observatories (e.g., TRACE, SoHO, Yohkoh), when taken together, give the spectral and spatial discrimination necessary for emission measure analysis of a range of coronal substructures. An examination of how specific substructures contribute to the full-disk averaged DEM can yield valuable insights for the interpretation of stellar coronae.

In this study we take an approach similar to that of Orlando et al. (2000,2001), Peres et al.(2000), Reale et al.(2001), and Drake et al. (2000). In this series of papers, they first probed the quality with which emission measure analysis can be done within the statistical and instrumental limits of Yohkoh/SXT data. With an emission measure reconstruction method tailored for Yohkoh data, they then investigated how DEMs of flares, background corona, and active region corona differed as compared to the full-disk DEM, and as seen through non-solar observatories such as the ROSAT/PSPC, EUVE, and ASCA/SIS. (see also Orlando et al. 2004 and Peres et al. 2004)

Here we discuss the application of a novel procedure with which we can use emission measures to examine the Sun as an X-ray star. We demonstrate that by using a combination of archival data from TRACE, Yohkoh/SXT, SoHO/EIT, SoHO/CDS, and GOES, we can compare the emission structure of individual spatially resolved features in the corona with emission measures spatially averaged over larger fields of view. DEMs are reconstructed using a Markov-Chain Monte-Carlo (MCMC) algorithm (Kashyap & Drake 1998) which is easily adapted to any combination of observations obtained through different filters and bandpasses. This flexibility allows us to maximally exploit the spatial and spectral coverage, as well as the resolving capability, of each of the instruments as necessary for the emission measure analysis of the individual coronal feature or larger field-of-view (FOV) in question. We present first results of emission measure reconstructions on contemporaneous solar data for the full-disk, an active region, and a FOV centered on a loop footpoint.

In §2, we list the datasets used in the analysis. We describe the DEM reconstruction method briefly in §3, and the describe our approach to the problem of multimission multi-instrument analysis in §4. The results of the analysis are detailed in §5 and summarized in §6.

Proc. 13th Cool Stars Workshop, Hamburg, 5–9 July 2004, F. Favata et al. eds.

2. DATA

We use the following datasets, all obtained on June 12, 1998:

– SoHO/EIT 171, 195 and 284, Å full-disk observations between the times 12:59 to 13:07 UTC
– Yohkoh/SXT Al.1 and AlMg full-disk observations between the times 13:48 to 23:59 UTC
– GOES8 and GOES9 full-disk soft & hard X-ray integrations from continuously monitoring ion-chamber detectors
– TRACE 171, 195, and 284 Å observations of AR 8238 between the times 12:05 to 23:55 UTC
– SoHO/CDS raster observations of a loop footpoint in AR8238 between the times 19:14 to 22:50 UTC

Observation durations range from 0.0173 s for Yohkoh/SXT to 152 s for SoHO/EIT. In the data reduction process we identify contemporaneous datasets, spatially match the observations, account for dark currents and flat fielding, remove particle hits, and cull for optimal exposure times.

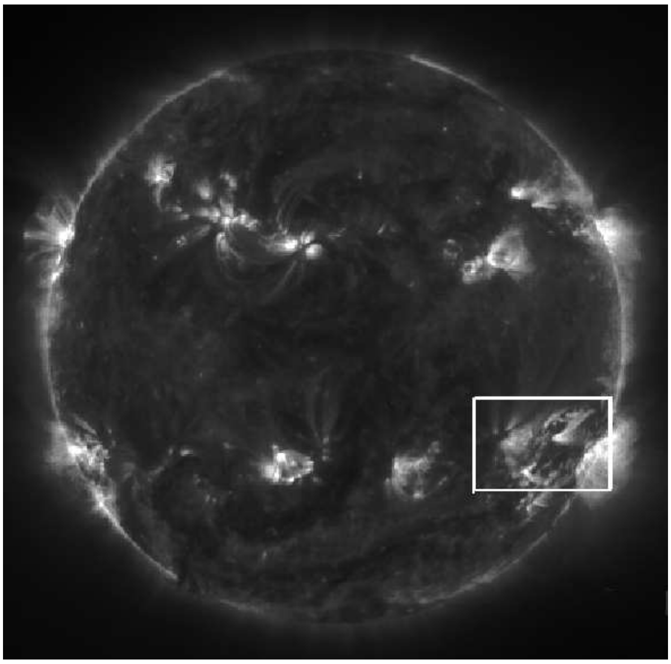

Figure 1. EIT 171 image of the full-disk. The TRACE AR image FOV is enclosed in a box.

3. Emission Measure reconstruction

A differential emission measure (DEM) is one of the basic ways of parameterizing the temperature structure of optically thin, collisionally dominated coronal plasmas. The DEM describes the amount of emitting plasma as a function of temperature. A DEM is obtained by inverting the equation:

$$I_{ul} \propto \int_T d\,\log T\; G_{ul}(T) n_e^2 \frac{dV(T)}{d\,\log T}, \qquad (1)$$

where the *Differential Emission Measure* is

$$DEM(T) = n_e^2 \frac{dV(T)}{d \log T}. \qquad (2)$$

When examining stellar spectra from, e.g., Chandra or XMM, I_{ul} are individual line intensities and $G_{ul}(T)$ are line contribution functions which include the line cooling emissivities, electron densities, and abundances. For solar imaging data, if I is the intensity measured in an instrument passband then $G(T)$ is an instrumental temperature response, which contains the effective area weighted $G(T)_{ul}$ of all the lines that contribute significantly to the observed signal.

$DEM(T)$ is not easily obtained by inverting Eqn 1. due to notorious instability in the integral equation. Kashyap & Drake (1998) offer a DEM reconstruction method based on a Markov-Chain Monte Carlo (MCMC) algorithm. The MCMC algorithm is a robust method widely used in statistical literature. When applied to the DEM inversion problem, the algorithm allows for the use of fluxes as upper limits, employs physically based smoothing criteria, produces an estimate of the uncertainties as a matter of course, and is easily customizable to different types of input data, including the use of line or filter ratios as

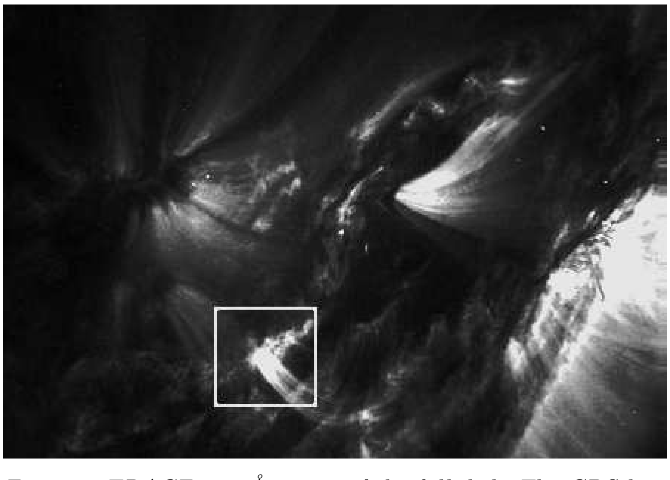

Figure 2. TRACE 171 Å image of the full-disk. The CDS loop footpoint image FOV is enclosed in a box.

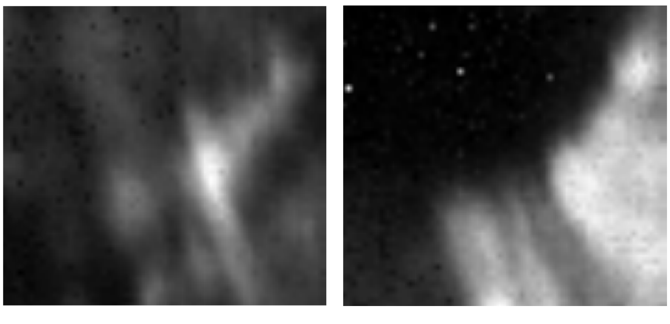

Figure 3. CDS Mg IX λ368.068 (left) and Fe XVI λ360.759 (right) images centered on a loop footpoint.

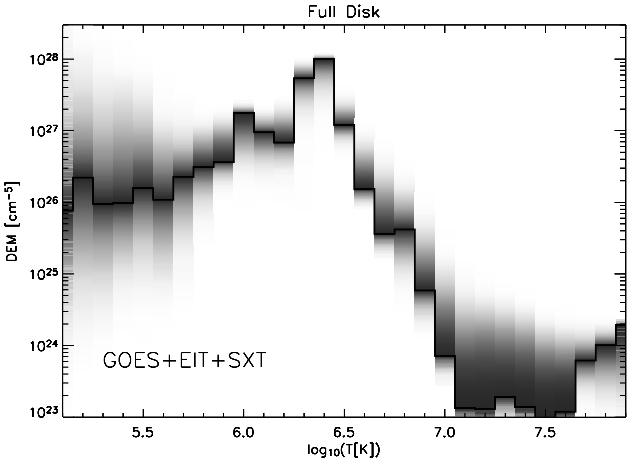

Figure 4. Reconstructed emission measure using EIT (171, 195, 284 Å), SXT (Al.1, Almg), and GOES (soft, hard) observations.

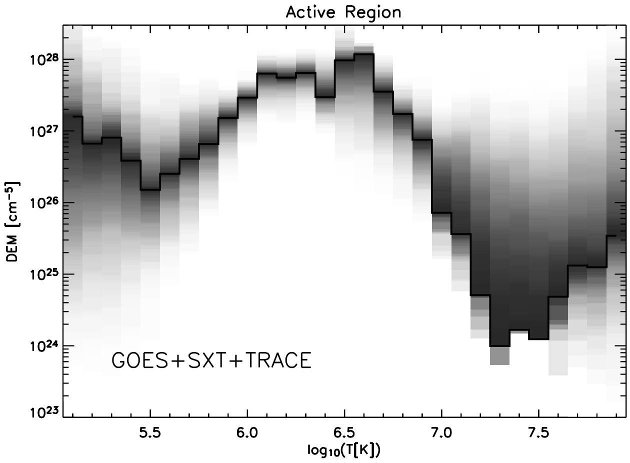

Figure 5. Reconstructed emission measure using TRACE (171, 195, 284 Å) images, cropped SXT (Al.1, AlMg) images, and GOES fluxes as upper limits.

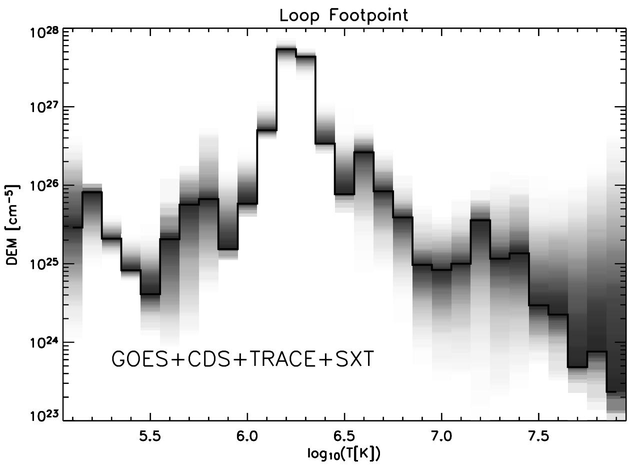

Figure 6. Reconstructed DEM using CDS (O V λ629.730, MG IX λ368.068, and Fe XVI λ360.759) raster images, cropped TRACE (171, 195, 284 Å) and SXT (Al.1, AlMg) images, and GOES fluxes as upper limits.

well as mixing together data from different instruments. Some of the drawbacks to the method are that it is generally slower than other methods, convergence must be evaluated on a case-by-case basis, and it cannot be used as a black box fitting engine. Also, as with all DEM reconstruction methods, there is no way of easily representing the errors on the DEM, e.g. as simple 1σ error bars.

MCMC DEM reconstruction is implemented in the Package for the Interactive Analysis of Line Emission (Kashyap & Drake 2000) (PINTofALE) [1].

4. Our Approach

We maximize temperature coverage by assembling contemporaneous and co-spatial data from archival observations. The analysis process can be summarized as three steps. First, we integrate fluxes over structures of interest, or even an entire FOV, to get an average count rate in each bandpass. Then we calculate temperature responses for each bandpass in PINTofALE using instrument calibration products from Solar Soft, the CHIANTI 4.2 atomic database (Young et al. 2003), solar abundances from Feldman (1992), and ionization equilibrium calculations from Mazzota et al. (1998). Lastly, we reconstruct spatially averaged DEMs using Markov-Chain Monte Carlo as implemented in PINTofALE.

5. Results

From temporal and spatial overlaps in the data sets available, three fields of view were determined to have the spectral coverage necessary to warrant an emission measure reconstruction via MCMC.

1. We have derived a full-disk averaged DEM (Figure 4) using full-disk EIT (171, 195, and 284 Å) Yohkoh/SXT (Al.1 and AlMg), and the GOES 9 (soft and hard) observations which provide adequate temperature coverage from $\log T \sim 6.0$ to $\log T \sim 8.0$ (see Figure 1).
2. A DEM averaged over a FOV centered on AR 8238 (Figure 5) was possible with TRACE 171, 195, and 284 Å observations, the full-disk SXT (Al.1 and AlMg) images cropped to the AR FOV, and the full-disk GOES soft and hard fluxes used as upper limits (Figure 2). These gave nominal temperature coverage from $\log T \sim 6.0$ to $\log T \sim 6.7$.
3. We have derived a third DEM averaged over a FOV centered on a loop foot point in AR 8238 (Figure 6) with CDS O V λ629.730, Mg IX λ368.068, and Fe XVI λ360.759 raster images, cropped TRACE (171, 195,

[1] The PINTofALE software suite written in Interactive Data Language (IDL), is designed for, but not limited to, the analysis of high resolution X-ray spectra. Basic functions include line identification, line fitting, and interaction with precompiled atomic databases. PINTofALE is freely available at: http://hea-www.harvard.edu/PINTofALE/ and can also be obtained through SolarSoft.

and 284 Å) and SXT (Al.1 and AlMg) images, and again using GOES fluxes as upper limits (Figure 3). This combination provides good temperature coverage from $\log T \sim 5.5$ to $\log T \sim 6.7$.

The full-disk DEM, as seen in Figure 4, peaks at $\log T = 6.4$. It has a slope of ~ 1.9 towards cooler T and drops off sharply after the peak towards higher T with a slope of ~ -5.0. The analysis of AR 8232 (covered by the TRACE FOV) shows a DEM that peaks at a hotter temperature of $\log T = 6.6$ with a slope of ~ 1.4 at cooler T and drops with a slope of ~ -2.4 towards higher T (Figure 5). The smallest region we explored, the CDS FOV focused on a loop footpoint, shows a nearly isothermal DEM (Figure 6) which peaks sharply at $\log T \sim 6.2$. The error bands in Figures 4-6 indicate the spread of the MCMC DEM simulations with the %50 best associated probabilities.

The slope of the DEM derived for AR 8232 matches that expected from hydrostatic loops (Rosner, Tucker, and Vaiana 1978; hereafter RTV). An RTV loop with a maximum temperature of $\log T = 6.6$ and the observed emission measure would be 2.0×10^{10} cm long, consistent with the loop sizes observed in the image (see Figure 2). Such a loop results in a footpoint with temperature $\log T = 6.2$ at a height of 6.1×10^{8} cm, consistent with the DEM derived for the smallest FOV (Figure 6).

The TRACE FOV image (Figure 2) and CDS FOV images (Figure 3) also show plage-like emission at the loop base. The emission measure distribution of this so called 'moss' (see Peres et al. 1994 and Martens et al. 2000) should be resolvable using the current data set. Our findings described above and the presence of 'moss' warrant further investigation using more spatial discrimination and other sets of co-spatial, contemporaneous data.

6. Summary

We have carried out a multi-instrument, multi-mission, reconstruction of the emission structure of the solar corona on June 12, 1998. We find a direct correspondence between features at different scales, and find that we can model the active region AR 8232 as being in RTV-style hydrostatic pressure balance.

The above results demonstrate the power of using imaging data over different filters for emission measure analysis. Within the limits of adequate spectral coverage and signal, we can examine in detail the emission measures of individual coronal features as well as the full-disk Sun as a star. We can now begin to de-construct the solar corona into a collection of coronal DEM building blocks, and examine how substructure emission measures can contribute to the full-disk averaged emission measure.

For the future, we plan to extend this study to a larger range of coronal features including flaring plasma and post-flare loops, as well as examine the emission measure signatures of different activity levels. Finally, we will apply solar results to observations of stars in order to better understand what types of structures might dominate the corona of different star types.

Acknowledgements

This work was made possible by the AISR grant NAG5-9322 which supports the development of the PINTofALE software suite. VLK and JJD were supported by NASA contract NAS8-39073 to the Chandra X-ray Center. EED, MW, and ALS were supported by AIA contract SP02D430IR to the Lockheed Martin Corp. We are grateful to Harry Warren, Amy Winebarger, and Richard Nightingale for assistance and helpful comments with data interpretation.

References

Drake J.J., Peres, G., Orlando S., Laming J.M., Maggio A. 2000, ApJ 547, 902

Feldman U. 1992, Phys.Scr 46, 202

Golub L. 1981, SAO Special Report 392, 39

Kashyap V.L., Drake J.J. 1998, ApJ 503, 450

Kashyap V.L., Drake J.J., BASI 28, 475

Martens P.C.H., Kankelborg, C.C., Berger T.E. 2000, ApJ 537, 471

Mazzotta P., Mazzitelli G., Colafrancesco S., Vittorio N. 1998, A&AS 133, 403

Orlando S., Peres G., Reale F. 2000, ApJ 528, 524

Orlando S., Peres G., Reale F. 2001, ApJ 528, 524

Orlando S., Peres G., Reale F. 2004, A&A 424, 677

Peres G., Rosner R., Serio S. Vaiana G.S. 1982, ApJ 252, 791

Peres G., Reale F., Golub L. 1994, ApJ 422, 412

Peres G., Orlando S., Reale F. 2000, ApJ 528, 537

Peres G., Orlando, S., Reale F. 2004, ApJ 612, 472

Reale F., Peres G., Orlando S. 2001, ApJ 557, 906

Rosner R., Tucker W. H., Vaiana G.S. 1978, ApJ 220, 643

Rosner R., Golub L., Vaiana G.S. 1985, ARA&A 23, 413

Young P. R., Del Zanna G., Landi E., Dere, K. P., Mason H. E., Landini, M. 2003, ApJSS 144, 135

Vaiana G.S., et al. 1981, ApJ 245, 163